PCCP

PAPER

View Article Online
View Journal | View Issue

Open Access Article. Published on 16 March 2023. Downloaded on 12/6/2025 1:20:20 PM.
This article is licensed under a Creative Commons Attribution 3.0 Unported Licence.

Check for updates

Cite this: *Phys. Chem. Chem. Phys.*, 2023, **25**, 9382

Paddle-wheel mechanism in doped succinonitrile–glutaronitrile plastic electrolyte: a joint magnetic resonance, dielectric, and viscosimetry study of Li ion translational and molecular reorientational dynamics

S. Lansab, *[a] B. Grabe [b] and R. Böhmer [a]

Received 12th December 2022,
Accepted 8th March 2023

DOI: 10.1039/d2cp05799a

rsc.li/pccp

Mixtures of 60% SN (succinonitrile) and 40% GN (glutaronitrile) doped with LiTFSI or $LiPF_6$ at different concentrations are investigated using dielectric spectroscopy. Room temperature conductivities up to 10^{-3} S cm^{-1} are measured along with an overall conductivity enhancement of almost five decades compared to pure SN. Additionally, the dynamics of the methylene (CD_2) groups of SN and that of the Li^+ ions within the mixture are studied in a wide temperature range using ^{2}H and ^{7}Li NMR relaxometry, respectively. Static-field-gradient proton NMR combined with viscosity measurements probe the molecular diffusion. GN addition and Li doping both enhance the electrical conductivity significantly, while leaving the reorientational motion within the matrix essentially unchanged. The times scales and thus the effective energy barriers characterizing the Li ion motion as well as the molecular reorientations are very similar in the liquid and in the plastic phases, findings that argue in favor of the presence of a paddle-wheel mechanism.

1. Introduction

In recent years, the need for powerful energy-storage solutions has become crucial for a more sustainable future, where fuel-based energy sources cease to be an option and where green energy is expected to play a major role. A transition to such a future requires efficient energy materials, hence the need for better electrolytes. These materials must satisfy several conditions, including electrochemical aspects, such as an ionic conductivity of at least 10^{-4} S cm^{-1} and a high electrochemical stability, as well as practical, safety-, and economy-related aspects.

Whether used as simple plasticizers among more complex systems or as main matrices, dinitriles such as $N{\equiv}C{-}(CH_2)_n{-}C{\equiv}N$ are subject to extensive research and have proven to be suitable electrolytes for Li ion batteries when doped with sufficient amounts of Li salt.[1–11] Their relatively high ionic conductivity, even in the absence of a dopant,[12] alongside with their low toxicity and low flammability, make them particularly compelling candidates for battery research.

Since dinitriles are highly polar and can dissolve enormously large amounts of Li salts,[13] when doped with Li ions they can reach room-temperature ionic conductivities of up to $\sigma \approx 10^{-3}$ S cm^{-1}.[3] On top of that, dinitriles show a large electrochemical stability window (up to 6 V *vs.* Li^+/Li)[6] and a better electrode/electrolyte interfacial resistance than conventional inorganic solid-state materials.[14] Compared with conventional polymer electrolytes, nitrile-based ion conductors require smaller amounts of doping and are easier to produce.

In that sense, succinonitrile (SN, $n = 2$) is particularly interesting for pliable or stretchable cells because it exhibits a plastically crystalline phase.[15–17] In this phase, its molecular constituents exhibit partial alignment arising from the orientational degrees of freedom that are located on well-defined lattice sites.[18] Thus, this electrolyte allows for a large degree of mechanical flexibility and high deformability. Additionally, Angell has shown that the temperature window in which the plastic phase exists, happens to be easily extendable by adding a sufficient amount of glutaronitrile (GN, $n = 3$).[19]

Moreover, Geirhos *et al.*[20] reported that the ionic conductivity of $LiPF_6$ doped SN increases by about 3 decades when adding GN. These authors observed a strong coupling between the ionic conductivity of the Li ions and the reorientational motion of the matrix molecules when increasing the GN fraction. These findings were suggested[20] to be compatible with the

[a] *Fakultät Physik, Technische Universität Dortmund, D-44221 Dortmund, Germany. E-mail: sofiane.lansab@tu-dortmund.de*
[b] *Fakultät für Chemie und Chemische Biologie, Technische Universität Dortmund, D-44221 Dortmund, Germany*

 This journal is © the Owner Societies 2023

Open Access Article. Published on 16 March 2023. Downloaded on 12/6/2025 1:20:20 PM. This article is licensed under a Creative Commons Attribution 3.0 Unported Licence.

previously discussed "revolving door mechanism",[21,22] also in mixtures of different other nitriles with SN.[23] The relevance of this mechanism in a wide range of different solid electrolytes and the exciting prospects this offers for the design of future materials was recently reviewed.[24]

Additionally, several studies provided valuable information regarding the structure of SN before and after Li ion incorporation.[18,25–32] In its plastic phase, SN crystallizes in a cubic structure with a lattice constant of a = 6.341 Å.[18] In particular, incorporation of salts such as $LiClO_4$ or lithium bis(trifluoromethanesulfonyl)imide (LiTFSI) does not alter this lattice spacing.[27] Furthermore, X-ray absorption spectroscopy at the Cu K-edge reveals that the cations (in CuTFSI doped SN) occupy well-defined sites in the cubic lattice. These are each coordinated by four SN molecules which "persists even in the molten host".[29] Furthermore, a variety of Li-ion solvation structures were identified in SN by means of combining ultrafast vibrational spectroscopy and quantum chemical investigations, where the latter reveal, *e.g.*, for a Li^+–SN_3 complex "that there are four possible conformations for one Li^+ directly binding to 3 SN molecules".[31] Taking the conformational changes into account, for the condensed phases one thus expects a large multiplicity of charge environments at the cationic sites.

Recently, Sasaki *et al.*[33] conducted molecular dynamics simulations of the Li ion transport within an SN matrix: These authors suggested a two-step migration process, where first, in the vicinity of a vacant Li site, a gauche-to-trans isomerization of two SN molecules takes place, followed by a swing motion by one of them "holding Li-ions towards the vacancy".[33]

Interestingly, for GN fractions on the order of 15%, Zachariah *et al.*[34] reported a breakdown of the correlation between reorientational motion and doping induced conductivity. Furthermore, these authors ascribed their findings to a conductivity process arising from the self-diffusion of a minority of ionized dinitrile molecules.

Finally, in nitrile materials the mutual distances between the sites participating in the Li ion exchange can be relatively long ($\approx$5 Å for $Li(N(SO_2F)_2)(SN)_2$),[36] while low activation energies against Li hopping have been reported.[12,35,36] The ionic transport mechanism causing these low activation energies is not fully understood, and deeper insights regarding the interactions governing the charge dynamics are needed to optimize wider applications. In particular, the relationship between the molecular reorientation of the nitrile molecules and the lithium hopping process requires further clarification.[37]

In this context, nuclear magnetic resonance (NMR) spectroscopy has established itself as a primary technique for the study of Li electrolytes.[38–43] Indeed, it has the advantage of being element specific, allowing for an independent investigation of the reorientational motion of the matrix, here through the nitrile molecules, as well as of the hopping motion of the Li ions that are involved in the conduction process. Therefore, if the Li ions within the SN–GN matrix occupy distinguishable environments, the Li spins resonate at different frequencies which then can be detected using suitable NMR experiments. The resulting distribution of the different resonance frequencies usually provides valuable information about the relevant interactions and thus on the nature of the charge transport process.

Furthermore, with the availability of perdeuterated SN ($SN\text{-}d_4$),[44] ^2H NMR can be exploited to directly probe the matrix dynamics through the reorientational fluctuations of the C–D bonds.[45] Additionally, one can use ^1H NMR to monitor the dynamic behavior[46] specifically of the GN molecules in the same binary system, for instance, by means of NMR diffusometry. This latter method, combined with viscosity measurements, provide deep insights into the type of dynamics occurring within the matrix and help to clarify how the addition of GN contributes to the overall conductivity enhancement.[20] Additionally, abrupt viscosity changes are useful to unravel the phase transitions of SN–GN mixtures.

Similarly, dielectric spectroscopy yields helpful information regarding the reorientational dynamics within the matrix. It is sensitive to the molecular (electric) dipole moment which for the dinitriles happens to be large (around 3.9 D for SN and GN).[47] The combination of dielectric and NMR spectroscopy as well as the combination of ^2H and ^7Li NMR thus can elucidate the possible correlation between reorientational motion and ionic charge transport.

Finally, based on the classification of correlated dynamics discussed by Jansen[22] and with the information obtained from the present NMR data in combination with dielectric and rheology results, we will provide a clarified picture on how the Li ions and the nitrile molecules dynamically cooperate.

In the present work, we investigate the ionic conductivity and reorientational dynamics of the plastic mixture of 60% SN and 40% GN doped with 1% and 5% of LiTFSI or $LiPF_6$. We use dielectric spectroscopy and viscosimetry as well as ^1H, ^2H, and ^7Li NMR. The dynamics of the Li ions as well as that of the matrix is thoroughly studied *via* deuterated SN. In addition, detailed comparisons with previous results[48–50] obtained for undoped 60SN–40GN mixtures are provided.

2. Experimental details

Protonated GN (stated purity 99%) and protonated SN (99%) as well as LiTFSI (99%), all purchased from Sigma-Aldrich, are used in this work. The deuterated SN (degree of deuteration: 91%) is from the previously used batch.[48] $LiPF_6$ (98%) was acquired from ThermoFischer Scientific. All samples were prepared inside a glovebox, where 60% SN and 40% GN were mixed as reported earlier.[48] The Li salts were first dried at T = 353 K for a minimum of 8 hours directly before use. Afterwards they were ground to optimize dissolution and added to the nitrile mixtures under heavy stirring. Karl Fischer titration showed water fractions of less than 0.05% for all investigated samples. After several freeze–thaw–pump cycles the NMR samples were flame sealed in glass tubes.

The ^7Li spectroscopy measurements were carried out using a home-built spectrometer operated at a Larmor frequency of 116.9 MHz. To record ^7Li solid-echo spectra, the 90° ^7Li pulse was 3 μs long. A Gaussian apodization with a spectral width of

Open Access Article. Published on 16 March 2023. Downloaded on 12/6/2025 1:20:20 PM.
This article is licensed under a Creative Commons Attribution 3.0 Unported Licence.

1 kHz was applied. The software package DMFit was used to analyze the spectra.[51] For ^{7}Li relaxometry, a saturation recovery pulse sequence followed by Hahn-echo or solid-echo refocusing was used.

NMR deuterium relaxometry and proton diffusion measurements were performed using home-built spectrometers operated at Larmor frequencies of 46.5 MHz for ^{2}H and 87.0 MHz for ^{1}H. Deuteron spin–lattice relaxation times T_1 were measured using an inversion recovery pulse sequence augmented by Hahn-echo or solid-echo rephasing. Deuteron spin–spin relaxation times T_2 were obtained by employing Hahn-echo or solid-echo pulse sequences. Static field-gradient NMR was used to probe the proton diffusion in the samples. These experiments were conducted in the fringe field of a superconducting magnet employing a constant gradient strength of $g = (34.1 \pm 0.2)$ T m^{-1} as described previously.[48]

The ^{7}Li diffusion experiments were performed with a Bruker Avance III HD Nanobay 400 MHz spectrometer equipped with a 5 mm RT BBFO smart probe using stimulated echoes including longitudinal eddy current delays with bipolar gradients and spoil pulses.[52] The probe's maximum gradient strength of about 0.5 T m^{-1} was calibrated using doped D_2O water (P/N Z10906), containing 1% H_2O, 0.1% $GdCl_3$, and 0.1% $^{13}CH_3OH$. The diffusion coefficients were determined by linearly varying the gradient strength in 16 steps between 10 and 80% of its maximum using gradient pulse lengths δ between 1.6 and 2.8 ms, diffusion delays Δ between 0.3 and 1 s, and a 90° ^{7}Li pulse of 9.0 μs.

Dielectric spectroscopy experiments were carried out in a Novocontrol system in combination with an Alpha impedance analyzer and a Quatro temperature controller. The frequency range from 10^{-1} to 10^6 Hz was scanned. The typical temperature stability was ±0.1 K.

Rotational viscosities were recorded in the liquid phase of the samples and in the linear-response regime using an Anton-Paar MCR 502 rheometer and an EVU20 temperature module at a typical temperature stability of ±0.2 K. The sample was placed between two plates separated by d = 0.9 mm. The upper plate rotates with an angular frequency ω_{rot} leading to a shear rate $\dot{\gamma} = \omega_{rot} r/d$, while the lower plate with a diameter of $2r$ = 50 mm is fixed.

3. Results and analyses

A. Dielectric spectroscopy

To probe the reorientational motion of the matrix and the conductivity enhancement after doping, we conducted dielectric spectroscopy measurements during cooling on three $(SN\text{-}d_4)_{0.6}(GN)_{0.4}$ mixtures: These were doped with 1% $LiPF_6$, 5% $LiPF_6$, or 5% LiTFSI. Ref. 37 presented modulus losses for samples with 5% LiTFSI doping, but neither conductivity nor permittivity were reported, two quantities that we find particularly useful for comparison with our NMR results. Furthermore, although dielectric data for 1% $LiPF_6$ doped $SN_{0.6}GN_{0.4}$ were presented in ref. 20, here we measured this sample to ensure a better overall comparability of our results also in view of the dependence on the Li salt concentration.

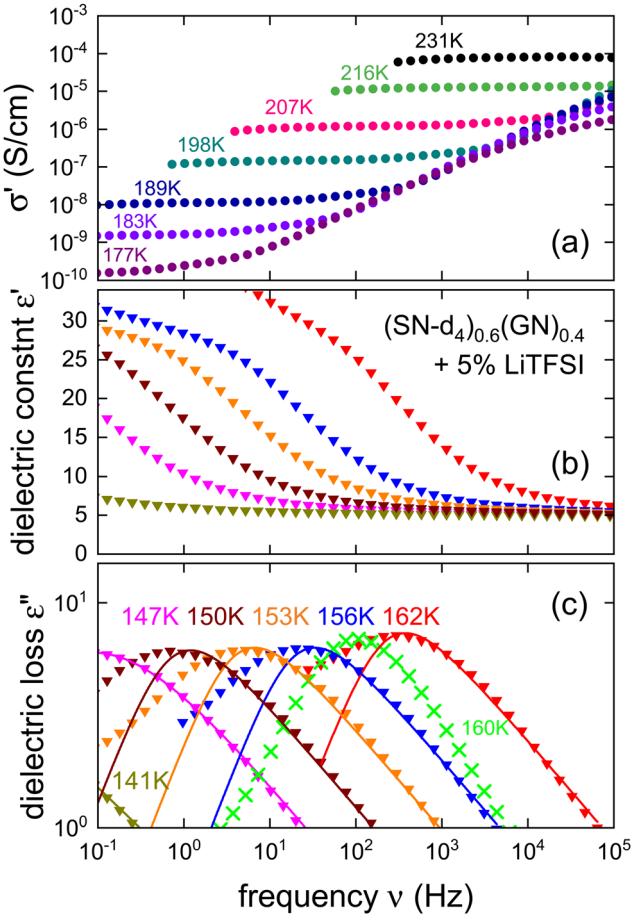

Fig. 1 Frequency-dependent measurements of (a) the electrical conductivity, (b) the real part, and (c) the imaginary part of the complex permittivity of $(SN\text{-}d_4)_{0.6}(GN)_{0.4}$ doped with 5% LiTFSI. The temperature range for frame (a) is between 213 and 177 K, while that for frames (b) and (c) is between 162 and 141 K. The crosses in frame (c) show dielectric losses for undoped $(SN\text{-}d_4)_{0.6}(GN)_{0.4}$,[48] acquired at T = 160 K. In this plot, these data are displayed with a relaxation strength that was rescaled by a factor of 0.22. The solid lines in frame (c) reflect fits using eqn (1) with $\gamma = 0.5 \pm 0.1$.

The results for the sample with 5% LiTFSI are presented in Fig. 1, where frame (a) shows the real part of the frequency dependent electrical conductivity $\sigma'(\nu)$, focusing on frequencies for which electrode polarization is not relevant. The dc conductivity corresponds to the plateau σ_{dc} observed in $\sigma'(\nu)$, which for T = 231 K appears near 10^{-4} S cm^{-1}. This value indicates an exceptionally high ionic conductivity. For the mixture without Li doping, at the same temperature we observed a dc plateau of about 10^{-7} S cm^{-1}.[48] This difference implies a LiTFSI doping induced conductivity enhancement of at least three decades, in agreement with that reported for similar mixtures doped with various other Li salts.[20,34] Towards lower temperatures, the plateau in σ' shifts to lower values and lower frequencies.

Fig. 1b and c show the frequency dependent dielectric constant ε' and the dielectric loss ε'', respectively, measured at various temperatures. As the frequency increases, the dielectric

 This journal is © the Owner Societies 2023

Open Access Article. Published on 16 March 2023. Downloaded on 12/6/2025 1:20:20 PM.
This article is licensed under a Creative Commons Attribution 3.0 Unported Licence.

constant ε' displays a steplike decrease from about 50 to 5, while between 162 and 147 K the dielectric loss ε'' reveals characteristic peaks in the present frequency window that originate from a reorientational relaxation process. These peaks shift to lower frequencies with decreasing temperature.

The decrease seen in the dc conductivity as well as that observed in the dielectric constant while the loss peaks shift towards lower frequencies, are well-known dielectric aspects of liquids and plastic crystals[53] and are similar to results obtained for the undoped mixture.[48,49]

For an analysis of the dielectric spectra, like before,[48] we use the Cole–Davidson (CD) function[54]

$$\varepsilon^*(\nu) = \varepsilon_\infty + \frac{\Delta\varepsilon}{[1 + (\mathrm{i}2\pi\nu\tau_{\mathrm{CD}})]^\gamma} + \frac{\sigma_{\mathrm{dc}}}{\mathrm{i}\omega\varepsilon_0}, \tag{1}$$

where ε_∞ is the high-frequency permittivity, τ_{CD} the characteristic time, and γ refers to the asymmetric broadening of the dielectric loss peaks. The electrical conductivity term, $\sigma_{\mathrm{dc}}/(\mathrm{i}\omega\varepsilon_0)$, takes the dc conductivity of the sample into account. From the parameters appearing in eqn (1) one can extract the time constants relating to the maximum in the dielectric loss according to[55]

$$\tau_{\max} = \tau_{\mathrm{CD}}\left[\sin\left(\frac{\gamma\pi}{2+2\gamma}\right)\Big/\sin\left(\frac{\pi}{2+2\gamma}\right)\right]. \tag{2}$$

From Fig. 1c it is obvious that the solid lines calculated using eqn (1) with $\gamma = 0.5 \pm 0.1$, fit only the high-frequency flanks of the peaks seen in the dielectric loss ε''. The low-frequency side features an additional contribution that is not observed in the absence of Li ions, but visible (see, *e.g.*, Fig. 2c of ref. 20) even for a doping level of 1%.

B. Lithium NMR spectroscopy

The measurement of the static ^{7}Li (spin $I = 3/2$) NMR spectra yields information about the environment surrounding the Li ions and the type of interactions involved in spectral broadening. In ^{7}Li NMR, the line shape is often governed by electrical quadrupole interactions and to a lesser extent by magnetic dipole–dipole interactions.[38] Fig. 2 shows temperature dependent ^{7}Li spectra for $(\mathrm{SN\text{-}d_4})_{0.6}(\mathrm{GN})_{0.4}$ doped with 5% LiTFSI. As the temperature increases, a successive line narrowing is observed. The contributions to the spectral shape were assessed for the spectrum recorded at $T = 155$ K: We fitted this spectrum with a superposition of a Lorentzian line (accounting for 54% of the total intensity) and a Gaussian contribution (accounting for the remaining 46%). The full width at half maximum (FWHM) of the dipolarly broadened central-transition ($-1/2 \leftrightarrow +1/2$) line is $\Delta\nu_{1/2} = 6$ kHz, while for the quadrupolarly broadened satellite spectrum, one has $\Delta\nu_{1/2} = 32$ kHz. The broad satellite lineshape indicates that it is caused by a superposition of several NMR lines. These arise from different structural environments in which the Li ions experience quadrupolar interactions of different strengths.

Fig. 3 summarizes the temperature dependent line widths, obtained from the solid-echo echo spectra. For their analysis, we use an equation first put forward by Bloembergen, Purcell, and Pound.[56,57] In the present context it is exploited with the goal to extract the correlation times describing the translational motion of the Li ions

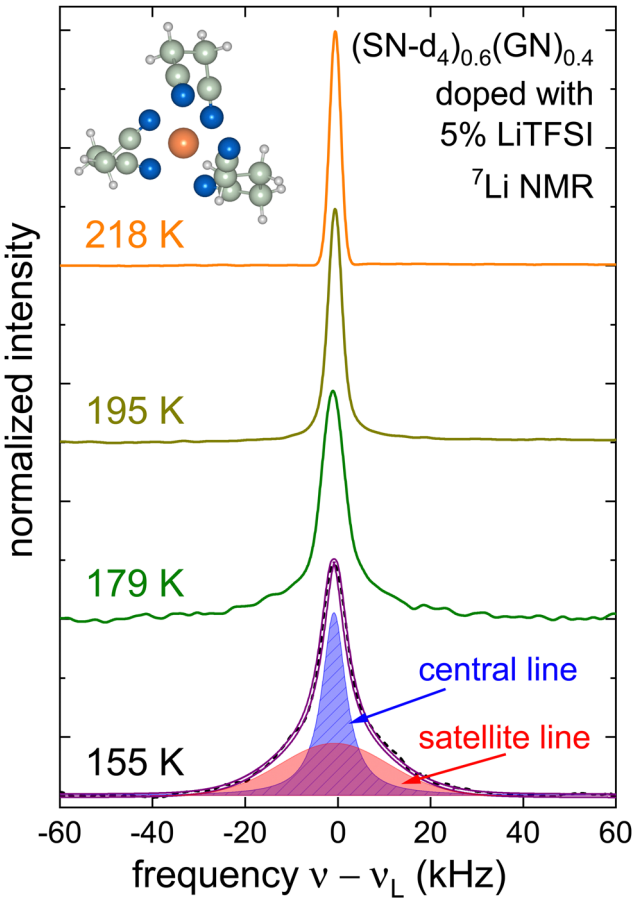

Fig. 2 ^{7}Li solid-echo spectra recorded for $(\mathrm{SN\text{-}d_4})_{0.6}(\mathrm{GN})_{0.4}$ doped with 5% LiTFSI. Note that for $T \geq 195$ K the spectra were recorded at 155.5 MHz, otherwise at 116.9 MHz. The spectrum obtained at 155 K (the measured spectrum is here shown as dashed line) was fitted with a superposition of a Lorentzian central-transition contribution (filled dashed area) and a Gaussian satellite-transition contribution (filled area without dashes). The sum of the two is represented by the solid purple double line. The inset shows a sketch, inspired by the structures in ref. 31, of a Li ion embedded in a solvation shell that features the partially negatively charged N atoms (blue spheres) of the dinitrile molecules.

$$\tau_{\mathrm{c}}(T) = \frac{1}{2\pi\,\alpha\,\Delta\nu(T)}\tan\left(\frac{\pi}{2}\frac{\Delta\nu^2(T)}{\Delta\nu_{\mathrm{RL}}{}^2}\right). \tag{3}$$

Here, $\Delta\nu(T)$ is the ^{7}Li central-transition line width, $\Delta\nu_{\mathrm{RL}}$ its rigid-lattice limit (≈ 8 kHz), and α a fit parameter (typically of order one, larger values were reported as well).[58] Eqn (3) is valid as long as the line broadening caused by the inhomogeneity of the magnet can be neglected ($T < 190$ K). Moreover, at $T < 170$ K the Li dynamics is slow on the time scale set by $1/\Delta\nu_{\mathrm{RL}}$ and the ^{7}Li central-transition line widths tend to saturate which also restricts the application range of eqn (3). The correlation times obtained for 170 K $< T <$ 190 K using this approach will be discussed in Section 4, below.

Open Access Article. Published on 16 March 2023. Downloaded on 12/6/2025 1:20:20 PM.
This article is licensed under a Creative Commons Attribution 3.0 Unported Licence.

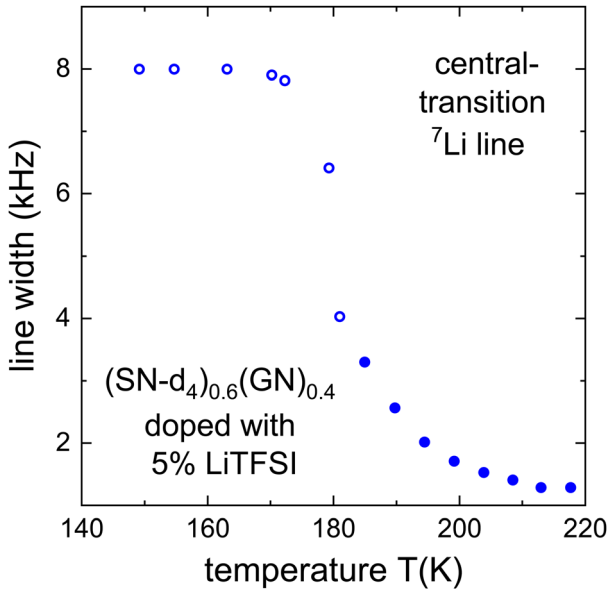

Fig. 3 ^{7}Li central-transition line widths determined for $(SN\text{-}d_4)_{0.6}(GN)_{0.4}$ doped with 5% LiTFSI at 155.5 MHz (filled symbols) and 116.9 MHz (open symbols).

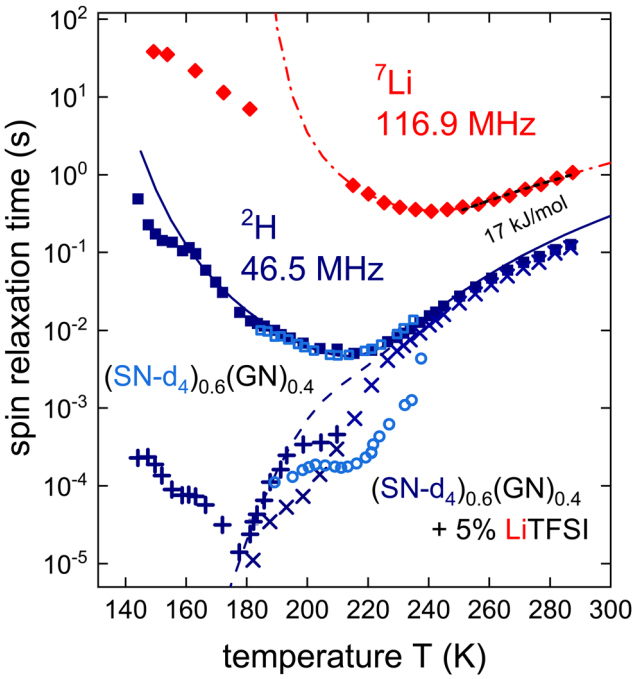

Fig. 4 The temperature dependent deuterium spin–lattice relaxation times T_1 (full symbols) and spin–spin relaxation times T_2 of $(SN\text{-}d_4)_{0.6}(GN)_{0.4}$ doped with 5% LiTFSI are shown. T_2 was measured using Hahn-echo (×, for $T > 180$ K) and solid-echo sequences (+, for $T < 210$ K). All measurements were recorded during cooling. The solid blue and dashed blue lines are calculated using eqn (7) in conjunction with the spectral density given by eqn (6) and using the fit parameters from ref. 48. Deuterium T_1 and T_2 data for the undoped mixture[48] are shown by the light blue squares and circles, respectively. ^{7}Li spin–lattice relaxation times for the doped mixture are presented as red diamonds. The dash-dotted red line is calculated using eqn (9) and the parameters given in the text. The black dashed line, *cf.* eqn (8), reflects an apparent energy barrier of 17 kJ mol^{-1}.

C. NMR relaxometry

In order to gain a detailed understanding of how the matrix dynamics is affected by adding Li ions, we conducted ^{2}H NMR relaxometry measurements on $(SN\text{-}d_4)_{0.6}(GN)_{0.4}$ doped with 5% LiTFSI. In fact, the reorientational motion within the matrix is predominantly due to isomerizations of the nitrile molecules[18,59] that are associated with fluctuations of the carbon–deuteron bonds. Thus, ^{2}H NMR directly monitors this reorientational motion within the matrix. In order to be sensitive to the charge carrier motion we exploited also ^{7}Li relaxometry.

We recorded the longitudinal magnetization recovery, $M_z(t)$, for the doped and the undoped samples and used the stretched exponential function

$$M_z(t) = M_0 + (M_i - M_0)\exp[-(t/T_1)^{\mu_1}], \tag{4}$$

for its parameterization. Here, t denotes the time after inversion or saturation and M_i and M_0 designate the initial and the equilibrium magnetization, respectively. The stretching of the spin–lattice relaxation is described by the Kohlrausch exponent μ_1.

Analogously, spin–spin relaxation times T_2 were acquired by varying the pulse separation Δ. The decay of the transverse magnetization $M_{xy}(\Delta)$ was parameterized using

$$M_{xy}(\Delta) = M_0 \exp[-(2\Delta/T_2)^{\mu_2}], \tag{5}$$

with the corresponding exponent μ_2.

The spin–lattice and spin–spin relaxation times for ^{2}H as well as the spin–lattice relaxation times for ^{7}Li, measured for $(SN\text{-}d_4)_{0.6}(GN)_{0.4}$ doped with 5% LiTFSI, are shown in Fig. 4. The corresponding Kohlrausch exponents were set to $\mu_1 = \mu_2 = 1$ for ^{2}H and ^{7}Li at $T > 160$ K and at $T > 180$ K, respectively.

For a quantitative analysis, we describe the orientational fluctuation probability of the C–D bond using the Cole–Davidson spectral density[60]

$$J_{CD}(\omega) = \frac{\sin[\gamma_{NMR}\arctan(\omega\tau_c)]}{\omega(1+\omega^2\tau_c^2)^{\gamma_{NMR}/2}}. \tag{6}$$

With the deuteron quadrupolar anisotropy parameter $^{2H}\delta_Q = \frac{3}{4}e^2qQ/\hbar$ and assuming that the quadrupolar relaxation mechanism dominates, the spin–lattice relaxation of the ^{2}H nuclei can be described as[61]

$$\frac{1}{^2T_1} = \frac{2}{15}{}^{2H}\delta_Q{}^2[J(\omega_L) + 4J(2\omega_L)] \tag{7}$$

and the ^{2}H spin–spin relaxation rate as[62]

$$\frac{1}{^2T_2} = \frac{1}{15}{}^{2H}\delta_Q{}^2[3J(\omega_Q) + 5J(\omega_L) + 2J(2\omega_L)], \tag{8}$$

where the quadrupolar frequency ω_Q is commonly defined as $\omega_Q = 2^{2H}\delta_Q$.

 This journal is © the Owner Societies 2023

Open Access Article. Published on 16 March 2023. Downloaded on 12/6/2025 1:20:20 PM.
This article is licensed under a Creative Commons Attribution 3.0 Unported Licence.

Analogously, the spin–lattice relaxation rate for ^{7}Li is[61]

$$\frac{1}{{}^7T_1} = \frac{2}{25}{}^{7\mathrm{Li}}\delta_\mathrm{Q}{}^2[J(\omega_\mathrm{L}) + 4J(2\omega_\mathrm{L})]. \tag{9}$$

Here, the ^{7}Li quadrupolar anisotropy parameter is defined as ${}^{7\mathrm{Li}}\delta_\mathrm{Q} = \frac{1}{2}e^2qQ/\hbar$.

Considering first the deuterium NMR data in Fig. 4, in the extreme-narrowing regime we observe a slight discrepancy between $^2T_1$ and $^2T_2$, similar to the behavior of the undoped mixture.[48] As previously reported, this discrepancy can be ascribed to deviations from local cubic ordering in the plastic phase.[44] A significant drop in $^2T_2$, but not in $^2T_1$, is observed near 230 K, *i.e.*, close to the temperature at which a related drop was observed for the undoped sample.[48] This observation is taken as a hint that the Li-doped sample is characterized by a somewhat lower transition temperature as compared to undoped $(\mathrm{SN\text{-}d_4})_{0.6}(\mathrm{GN})_{0.4}$.

To describe the relaxometry data, the blue lines in Fig. 4 were calculated using eqn (6), (7), and (8) in conjunction with γ_NMR = 0.3 and the time scale parameters found for undoped $(\mathrm{SN\text{-}d_4})_{0.6}(\mathrm{GN})_{0.4}$.[48] The ^{2}H quadrupolar anisotropy parameter turned out to be ${}^{2\mathrm{H}}\delta_\mathrm{Q} = 2\pi \times 125$ kHz, similar to the value determined for the undoped mixture.[48] Eqn (7) provides a good fit for the measured $^2T_1$, with small deviations observed at high temperatures. On the other hand, between 230 and 195 K the $^2T_2$ values deviate significantly from the fit based on eqn (8). Furthermore, $^2T_2$ displays a minimum near 175 K. All these findings agree excellently with those for the undoped sample and imply a complete absence of any kind of hindrance or stimulation of the molecular reorientation dynamics upon doping the matrix with 5% of Li salt.

Taking a closer look at the ^{7}Li spin–lattice relaxation times, these are seen to reveal a minimum near 240 K and to pass continuously through the liquid-to-plastic-crystal transition. The minimal $^7T_1$ is almost two decades longer than the minimal $^2T_1$. This difference for the different probe nuclei is compatible with our finding that the ^{7}Li quadrupolar interaction is significantly smaller than that observed for deuterium. The red line in Fig. 4 was calculated using eqn (6) and (9) in conjunction with γ_NMR = 0.24. The time scales were calculated using the Vogel-Fulcher parameters reported in ref. 48, with a pre-exponential factor of $\tau_\infty = 9.3 \times 10^{-12}$ s, a strength parameter D_τ = 2.1, and a divergence temperature T_0 = 178 K. These parameters are close to those reported by Davidowski *et al.*[37] for the same sample. The fit shown in Fig. 4 was found to agree well with the data when choosing ${}^{7\mathrm{Li}}\delta_\mathrm{Q} = 2\pi \times 32$ kHz, a value that is compatible with the width obtained from the ^{7}Li spectrum.

The ^{7}Li spin–lattice relaxation is governed by the quadrupolar interactions of the Li nuclei with their charge environment which is modulated in time. This modulation happens mostly as the ions perform translational motion within the SN–GN matrix and to a lesser extent, see Section 4, below, *via* conformational changes of adjacent dinitrile molecules.

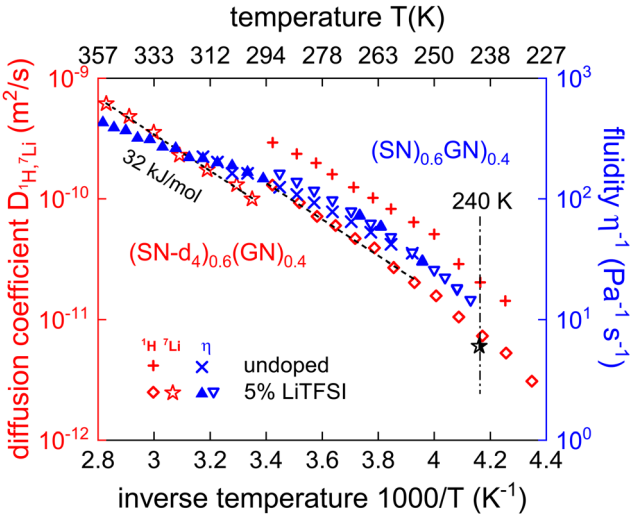

Fig. 5 Arrhenius plot of the temperature dependent ^{7}Li (unfilled red stars) and ^{1}H (unfilled red diamonds) self-diffusion coefficients (scale on the left-hand side) as well as of the temperature dependent fluidity, *i.e.*, of the inverse zero-shear viscosity (triangles, scale on the right-hand side). The unfilled red stars refer to measurements conducted during heating and using PFG NMR. The blue triangles pointing down or up refer to viscosity measurements taken upon cooling or heating, respectively. The half-filled black star refers to the ^{7}Li diffusion coefficient obtained from eqn (10), where τ_Li was obtained from the ^{7}Li T_1 minimum, using 1.8 Å as jump distance. Prior to each diffusion measurement, the samples were given 3 hours to equilibrate. ^{1}H self-diffusion coefficients and fluidities for the same mixture without doping[48] are shown by red (+) and blue (×) symbols, respectively. The dashed black lines reflect apparent energy barriers of 32 kJ mol^{-1}. The dash-dotted vertical line highlights the transition temperature from the undoped liquid to the plastically crystalline phase as identified in ref. 48.

Thus, by using the condition $\omega_0\tau_\mathrm{c} \approx 0.62$ (or slightly different for a Cole–Davidson distribution[63]), from the motional correlation time, τ_c at 240 K the Li-ion jump rate is estimated to be about $\tau_\mathrm{Li} = 12 \times 10^8$ s^{-1}. Based on the Einstein–Smoluchowski equation[64]

$$D_\mathrm{Li} = \frac{a^2}{6\tau_\mathrm{Li}}, \tag{10}$$

and using $D_\mathrm{Li} \approx 6 \times 10^{-12}$ m^2 s^{-1} as extrapolated from the high temperature data to 240 K (see Fig. 5), we estimate the jump distance of the Li ions to be 1.8 Å.

Finally, using the Arrhenius law, the activation energy for temperatures above the T_1 minimum turned out to be E_a = 17 kJ mol^{-1}, a value within the range of those reported for LiTFSI in GN.[65]

D. Diffusometry and viscometry

To selectively investigate the diffusion process of the GN molecules after addition of the Li ions, we measured the proton diffusion coefficient D of $(\mathrm{SN\text{-}d_4})_{0.6}(\mathrm{GN})_{0.4}$ doped with 5% LiTFSI. In other words, here (since SN contributes only ≤9% of the protons in our samples) we almost exclusively probe the diffusion of the GN molecules within the mixture. For that purpose, like in previous work,[48] we use a *static* field gradient

Open Access Article. Published on 16 March 2023. Downloaded on 12/6/2025 1:20:20 PM.
This article is licensed under a Creative Commons Attribution 3.0 Unported Licence.

and measure D by means of the stimulated-echo pulse sequence $\pi/2 - t_p - \pi/2 - t - \pi/2 - t_p$ – acquisition. Not writing out the spin relaxation terms, the resulting NMR signal is given by[66]

$$M(t) = M_0 \exp\left[-\gamma_H{}^2 g^2 t_p{}^2 (t + \tfrac{2}{3}t_p) D\right]. \quad (11)$$

Here, γ_H is the gyromagnetic ratio of the proton and g the gradient strength.

To probe the diffusion process not only of the matrix molecules, but of the charge carriers as well, we conducted temperature dependent ^{7}Li pulsed field gradient (PFG) NMR measurements on fully protonated $SN_{0.6}GN_{0.4}$ doped with 5% LiTFSI. In this experiment the stimulated-echo pulse sequence is used as well. The field gradient is incremented stepwise, thus causing an attenuation of the echo signal according to the Stejskal–Tanner equation[67]

$$M = M_0 \exp\left[-\gamma_{Li}{}^2 g^2 \delta^2 (\Delta - \tfrac{1}{3}\delta) D_{Li}\right]. \quad (12)$$

Here, γ_{Li} and D_{Li} are the lithium gyromagnetic ratio and the diffusion coefficient, respectively, δ is the duration of each PFG and Δ the time interval between two PFGs.

In addition to the diffusion measurements, we conducted temperature dependent zero-shear viscosity measurements on protonated $SN_{0.6}GN_{0.4}$ doped with 5% LiTFSI. The results for the ^{1}H and the ^{7}Li diffusion coefficients as well as for the fluidity (inverse of viscosity), presumably all referring to the liquid state, are shown in Fig. 5. For comparison, we also include results for undoped samples where some data could also be gathered in the plastic solid.[48]

From Fig. 5, it is clear that the proton diffusion of the dinitrile molecules slows down only slightly when adding the lithium salt. The measured viscosities confirm this trend, since they are similar to those obtained for the undoped mixture.[48]

When extrapolated to 294 K, the lithium diffusion coefficients differ by only a factor of 0.6 from those characterizing the dinitrile molecules. Furthermore, near room temperature the (effective) energy barrier of E_a = 32 kJ mol^{-1} that characterizes the lithium-ion diffusion agrees with the barrier deduced from the proton data.

A similar value can also be deduced for undoped $SN_{0.6}GN_{0.4}$.[48] Evidently, after doping the $SN_{0.6}GN_{0.4}$ mixture with 5% LiTFSI we do not observe an increase of E_a (*cf.* the dashed lines in Fig. 5) which reflects the activation barrier that a GN molecule has to overcome in order to undergo translational motion. This confirms that the nitrile diffusion, or at least that of the GN molecules, is barely affected by Li ion doping.

By contrast, based on terahertz time-domain spectroscopy for SN doped with various Li salts (including LiTFSI), Nickel *et al.*[35] observed a significant increase of the activation energy relative to that of pure SN. This increase was explained by "the presence of the effectively motionless ionic impurities".[35]

4. Discussion

To allow for deeper insights into possible correlations between the reorientational motion of the nitrile molecules and the overall charge transport, we compare the temperature dependent ionic conductivities (Fig. 6a) with the temperature dependent reorientational relaxation times τ (Fig. 6b) for the three currently investigated samples.

The conductivities were obtained from the dc plateaus in $\sigma'(\nu)$ (Fig. 1a), while the correlation times were extracted from the dielectric loss peaks (Fig. 1c), *i.e.*, by fits using eqn (1)

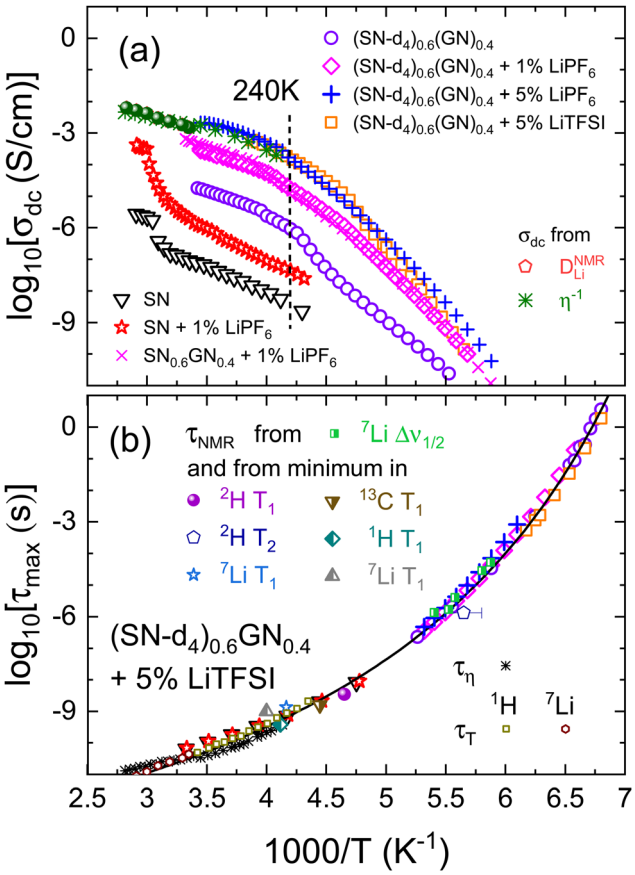

Fig. 6 Arrhenius plot of (a) the temperature dependent ionic conductivity and (b) the correlation time τ of $(SN\text{-}d_4)_{0.6}GN_{0.4}$ mixtures doped with 1% $LiPF_6$, 5% $LiPF_6$, and 5% LiTFSI from the present work. The data in frames (a) and (b) for pure SN (▽),[1] for SN doped with 1% $LiPF_6$ (☆),[23] for $(SN\text{-}d_4)_{0.6}(GN)_{0.4}$ (o),[48] and for another data set of $(SN)_{0.6}(GN)_{0.4}$ doped with 1% $LiPF_6$[20] (represented as magenta crosses ×) are from the literature. Frame (a) also includes the conductivities of $(SN\text{-}d_4)_{0.6}(GN)_{0.4}$ doped with 5% LiTFSI as obtained after converting the Li diffusion coefficients (*) and the fluidity (⬠): The conversions are based on eqn (13) and (14), respectively, and the parameters given below these equations. The vertical dotted line indicates the transition temperature (T = 240 K) of undoped $SN_{0.6}GN_{0.4}$.[48] Frame (b) includes correlation times from ^{2}H and ^{7}Li relaxometry of $(SN\text{-}d_4)_{0.6}(GN)_{0.4}$ doped with 5% LiTFSI, *cf.* Fig. 4 and from the ^{7}Li line widths $\Delta\nu_{1/2}$ (*cf.* Fig. 3). NMR time scales from Davidowski *et al.* for fully protonated samples are included as half-filled symbols.[37] The solid line represents a Vogel-Fulcher fit for undoped $(SN\text{-}d_4)_{0.6}GN_{0.4}$.[48] The shear relaxation times τ_η are obtained from the Maxwell relation $\tau_\eta = \eta/G_\infty$, with G_∞ set to 0.18 GPa. The translational times τ_T were obtained from eqn (15) and the hydrodynamic radius given below that equation.

Open Access Article. Published on 16 March 2023. Downloaded on 12/6/2025 1:20:20 PM.
This article is licensed under a Creative Commons Attribution 3.0 Unported Licence.

combined with eqn (2). For comparison, Fig. 6 includes data for pure SN,[1] for SN doped with 1% $LiPF_6$,[23] and for $(SN\text{-}d_4)_{0.6}(GN)_{0.4}$.[48] We also added the characteristic timescales obtained from ^2H and ^7Li NMR relaxometry of $(SN\text{-}d_4)_{0.6}(GN)_{0.4}$ doped with 5% LiTFSI, *cf.* Fig. 4.

Carefully reviewing Fig. 6a, it becomes obvious that the addition of 40% GN to pure SN enhances the conductivity by more than two decades, in accord with previous work.[20] Further addition of lithium salt leads to even higher conductivities with an overall enhancement of more than four decades, as compared to pure SN.[1] From Fig. 6a one observes similar conductivities no matter whether the samples are doped with $LiPF_6$ or with LiTFSI. In view of the environmental and health issues related to $LiPF_6$ it is clear that LiTFSI provides a safer alternative.

In order to compare the conductivity data obtained from dielectric spectroscopy with those deduced from the Li NMR diffusion coefficients and the viscosities shown in Fig. 5, we use the Nernst–Einstein relation,

$$\sigma_{dc,NMR} = D^{\sigma}\frac{n_{doped}q^2}{k_B T} = \frac{D_{Li}^{NMR}}{H}\frac{n_{doped}q^2}{k_B T}. \quad (13)$$

In this expression, n_{doped} (=2.4 × 10^{24} m^{-3}) is the charge-carrier number density of $(SN\text{-}d_4)_{0.6}GN_{0.4}$ doped with 5% LiTFSI and q refers to the elementary charge (here: of the Li^+ ion). Furthermore, eqn (13) defines the Haven ratio H which is a measure for the correlation among ionic motions[68] or after suitable adaption also among uncharged moieties.[69] For simplicity in the following we set $H = 1$. Analogously, by combining eqn (13) with the Stokes–Einstein relation, $D_\eta = k_B T/(6\pi\eta R_H)$,[64] for the fluidity of the doped mixture one obtains

$$\sigma_{dc,\eta} = \eta^{-1}\frac{n_{undoped}q^2}{6\pi R_H}. \quad (14)$$

Here, R_H designates the effective hydrodynamic radius and $n_{undoped}$ the charge-carrier number density of undoped $(SN\text{-}d_4)_{0.6}GN_{0.4}$. Applying the above expressions, in ref. 48 the values for R_H and $n_{undoped}$ were reported to be 1.0 Å and 8 × 10^{23} m^{-3}, respectively.

The conductivity obtained from eqn (13) can be understood as arising *exclusively* from the translational motion of the Li ions within the matrix. Eqn (14), on the other hand, considers a conductivity arising from the fluidity-related displacement of the nitrile molecules. From Fig. 6a one recognizes that the conductivities obtained from the Li diffusion *via* eqn (13) and from the viscosity measurements *via* eqn (14), nicely agree with each other and with the conductivities that are directly obtained from dielectric spectroscopy. These observations which essentially refer to the liquid phase imply a strongly correlated motion between the Li ions and the dinitrile molecules, a feature which results in a high ionic mobility and a significant conductivity enhancement.

Also referring to the liquid state, Fig. 6b includes viscosity-based timescales τ_η as assessed from the Maxwell relation, $\eta = G_\infty\tau_\eta$, where G_∞ is the high-frequency shear modulus. The value of G_∞ needed to achieve overlap (0.18 GPa) equals the one reported for the undoped mixture,[48] reinforcing the argument that the matrix properties are not affected by doping.

Furthermore, the correlation times τ_{NMR} from deuteron NMR and the ^1H diffusion based translational timescales

$$\tau_T = R_H^2/(9D), \quad (15)$$

agree well with the reorientational relaxation times obtained from dielectric spectroscopy when choosing R_H = 2.4 Å. This value is smaller than the ^1H diffusion-based estimate obtained for undoped $(SN\text{-}d_4)_{0.6}GN_{0.4}$ (3.4 Å),[48] but similar to the calculated van der Waals radius of GN (2.88 Å).[70]

Adapting eqn (15), ^7Li diffusion-based translational timescales are similarly calculated using R_H = 2.0 Å. Based on this value, the translational timescales turn out to agree well with the reorientational dynamics of the liquid matrix. The finding that the Li ion and the nitrile dynamics take place on the same time scale corroborates the scenario of an intimate coupling of the different degrees of freedom.

Additionally, by looking at Fig. 6b it becomes obvious that the reorientational correlation times of all Li doped samples are governed by the same molecular dynamics which agrees with that observed for the undoped SN–GN mixture.[48,49] Also the reorientational timescales reported for pure and doped SN crystals are the same.[1,20] All these findings clearly show that a few percent of Li doping do not affect the dynamics of the matrix. This supports the notion that, at the current doping levels, Li ion addition does not significantly distort the dinitrile lattice.

It is now important to realize that the ^7Li spin–lattice relaxation times vary smoothly across the crystallization transition and that the correlation times in the plastic phase inferred from $\Delta\nu_{1/2}$, using eqn (3) with α = 10, nicely coincide with the reorientational timescales, see Fig. 6b. These findings strongly suggest that the agreement of translational and reorientational timescales, above established for the liquid, persists also in the plastic solid. The relative large value of α deserves a comment: It may be conjectured that this could be a consequence of the circumstance (briefly mentioned in Section 3.C, above) that the frequency of the Li probe can be modulated (1) by active environmental changes stemming from the translation of the Li ions and to some extent also (2) by passive changes stemming from reorientations of adjacent nitrile segments, even if the Li ions would remain immobile.

However, in view of the multiplicity of nitrile configurations that characterizes the cationic solvation shell,[31] – and akin to the scenario theoretically treated and experimentally tested in ref. 71 for other solid Li ion conductors – the frequency modulation amplitude associated with the two kinds of situation differs vastly: (1) can be read here to imply that after a Li ion has jumped to another site, the orientations of essentially all its adjacent C≡N segments have changed at once. Typically, this will alter the NMR frequency of the Li probe significantly. (2) Conversely, a reorientation of only a single adjacent C≡N segment will change the NMR frequency of the Li probe by only a small step, unless the local reorientational

Open Access Article. Published on 16 March 2023. Downloaded on 12/6/2025 1:20:20 PM.
This article is licensed under a Creative Commons Attribution 3.0 Unported Licence.

motion is by itself highly cooperative. For $(SN)_{0.6}(GN)_{0.4}$ this appears not to be the case at least down to about 175 K.[72]

Ionic mobilities that are coupled with reorientational molecular motions were previously variously referred to as being indicative for a revolving-door or a paddle-wheel mechanism.[22,23,73] Often these terms are used indistinctively, however, they describe two different processes. Indeed here, the paddle-wheel mechanism implies cooperative dynamics between the reorientational motion of the dinitrile molecules and the hopping motions of the Li ions.[22] This leads to very similar time scales and thus effective activation energies for the rotational and translation degrees of freedom. As a prerequisite this mechanism requires the availability of sufficiently large free volume for the molecules to rotate.[74] The revolving-door mechanism, can be related to a scenario where the reorienting matrix molecules "react with an evasive motion towards the passage of cations".[22] Applied to the presently considered materials, this would imply just a correlated motion of Li ions and dinitrile molecules in the sense that only the temperature dependence of the corresponding times is the same but not the timescales themselves.

It is a remarkable finding that neither GN addition nor Li doping lead to any kind of hindrance or stimulation of the reorientational motion of the SN molecules. Considering the Li ions within a paddle-wheel scenario, this finding means that the ions occupy the free space between the dinitrile molecules without disturbing their reorientational motions. Furthermore, since the addition of GN does not affect the dynamics of the matrix but leads to higher conductivities, a possible explanation is that in the plastic phase, the addition of GN only affects the vacant space within the lattice of the mixed crystal. This way, the GN molecules would increase the free volume that is effectively available for Li ion migration, thus enhancing the efficiency of the charge transport. This hypothesis, here arrived at on the basis of dielectric spectroscopy, viscometry, and several NMR techniques, corroborates the interpretation of the very efficient charge transport in the nitriles in terms of a paddle-wheel and not just in terms a revolving-door mechanism.[20]

5. Conclusions

In this work we studied $(SN\text{-}d_4)_{0.6}(GN)_{0.4}$ doped with 5% LiTFSI using several experimental methods. For comparison we measured the electrical conductivity also for several other Li-salt doped nitriles. The conductivities deduced from the Li translational diffusion as well as those obtained from the viscosity measurements, agree with those measured using dielectric spectroscopy. A strong correlation of timescales and thus of the effective energy barriers deduced thereof, were found between the reorientational motion of the dinitrile molecules and the translational motion of the Li ions. To describe this correlation – based on the classification of correlated dynamics put forward by Jansen[22] and in harmony with the distinction of the terms given above – we identify the mechanism active in our sample as a "paddle-wheel" rather than a "revolving-door" mechanism.

Additionally, and independent of the type or of the amount of Li doping as well as of the addition or not of GN molecules, the reorientational dynamics of the nitrile molecules remain unaffected. Based on these findings, one is tempted to argue that volume defects that are present within the SN lattice, directly impact on the efficiency of the Li ion transport mechanism. Future structural investigations should be directed at further elucidating the correlation between the fraction of volume defects within the matrix and the overall efficiency of the paddle-wheel mechanism also when varying the size of the cationic species.

Conflicts of interest

There are no conflicts of interest to declare.

Acknowledgements

We thank Henrik Scholz (Department of Biochemical and Chemical Engineering, TU Dortmund University) for conducting Karl Fischer titrations and DSC measurements. This work was financially supported by the Deutsche Forschungsgemeinschaft under Project No. 429918288.

References

1 S. Long, D. R. MacFarlane and M. Forsyth, Fast ion conduction in molecular plastic crystals, *Solid State Ionics*, 2003, **161**, 105–112.
2 P.-J. Alarco, Y. Abu-Lebdeh, A. Abouimrane and M. Armand, The plastic-crystalline phase of succinonitrile as a universal matrix for solid-state ionic conductors, *Nat. Mater.*, 2004, **3**, 476–481.
3 A. Abouimrane and I. J. Davidson, Solid Electrolyte Based on Succinonitrile and LiBOB: Interface Stability and Application in Lithium Batteries, *J. Electrochem. Soc.*, 2007, **154**, A1031–A1034.
4 A. Abouimrane, P. S. Whitfield, S. Niketic and I. J. Davidson, Investigation of Li salt doped succinonitrile as potential solid electrolytes for lithium batteries, *J. Power Sources*, 2007, **174**, 883–888.
5 L.-Z. Fan, Y.-S. Hu, A. J. Bhattacharyya and J. Maier, Succinonitrile as a Versatile Additive for Polymer Electrolytes, *Adv. Funct. Mater.*, 2007, **17**, 2800–2807.
6 Y. Abu-Lebdeh and I. Davidson, High-Voltage Electrolytes Based on Adiponitrile for Li-Ion Batteries, *J. Electrochem. Soc.*, 2009, **156**, A60–A65.
7 N. Voigt and L. van Wüllen, The Effect of Plastic-Crystalline Succinonitrile on the Electrolyte System PEO:$LiBF_4$: Insights from Solid State NMR, *Solid State Ionics*, 2014, **260**, 65–75.
8 G. P. Pandey, T. Liu, C. Hancock, Y. Li, X. S. Sun and J. Li, Thermostable gel polymer electrolyte based on succinonitrile and ionic liquid for high-performance solid-state supercapacitors, *J. Power Sources*, 2016, **328**, 510–519.
9 D. Farhat, J. Maibach, H. Eriksson, K. Edström, D. Lemordant and F. Ghamouss, Towards high-voltage Li-ion

 This journal is © the Owner Societies 2023

Open Access Article. Published on 16 March 2023. Downloaded on 12/6/2025 1:20:20 PM.
This article is licensed under a Creative Commons Attribution 3.0 Unported Licence.

batteries: Reversible cycling of graphite anodes and Li-ion batteries in adiponitrile-based electrolytes, *Electrochim. Acta*, 2018, **281**, 299–311.

10 J. Villarreal, R. Orrostieta Chavez, S. A. Chopade, T. P. Lodge and M. Alcoutlabi, The Use of Succinonitrile as an Electrolyte Additive for Composite-Fiber Membranes in Lithium-Ion Batteries, *Membranes*, 2020, **10**, 45–58.

11 J. Möller, V. Van Laack, K. Koschek, P. Bottke and M. Wark, Solid-State NMR Revealing the Impact of Polymer Additives on Li-Ion Motions in Plastic-Crystalline Succinonitrile Electrolytes, *J. Phys. Chem. C*, 2023, **127**, 1464–1474.

12 S. Long, D. R. MacFarlane and M. Forsyth, Ionic conduction in doped succinonitrile, *Solid State Ionics*, 2004, **175**, 733–738.

13 Y. Ugata, R. Tatara, K. Ueno, K. Dokko and M. Watanabe, Highly concentrated $LiN(SO_2CF_3)2$/dinitrile electrolytes: Liquid structures, transport properties, and electrochemistry, *J. Chem. Phys.*, 2020, **152**, 104502.

14 H. Zhi, L. Xing, X. Zheng, K. Xu and W. Li, Understanding How Nitriles Stabilize Electrolyte/Electrode Interface at High Voltage, *J. Phys. Chem. Lett.*, 2017, **8**, 6048–6052.

15 G. Lee, J. W. Kim, H. Park, J. Y. Lee, H. Lee, C. Song, S. W. Jin, K. Keum, C.-H. Lee and J. S. Ha, Skin-Like, Dynamically Stretchable, Planar Supercapacitors with Buckled Carbon Nanotube/Mn–Mo Mixed Oxide Electrodes and Air-Stable Organic Electrolyte, *ACS Nano*, 2018, **13**, 855–866.

16 P. Lv, Y. Li, Y. Wu, G. Liu, H. Liu, S. Li, C. Tang, J. Mei and Y. Li, Robust Succinonitrile-Based Gel Polymer Electrolyte for Lithium-Ion Batteries Withstanding Mechanical Folding and High Temperature, *ACS Appl. Mater. Interfaces*, 2018, **10**, 25384–25392.

17 P. Lv, J. Yang, G. Liu, H. Liu, S. Li, C. Tang, J. Mei, Y. Li and D. Hui, Flexible solid electrolyte based on UV cured polyurethane acrylate/succinonitrile-lithium salt composite compatibilized by tetrahydrofuran, *Composites, Part B*, 2017, **120**, 35–41.

18 P. Derollez, J. Lefebvre, M. Descamps, W. Press and H. Fontaine, Structure of succinonitrile in its plastic phase, *J. Phys.: Condens. Matter*, 1990, **2**, 6893–6903.

19 C. A. Angell, Relaxation in liquids, polymers and plastic crystals—strong/fragile patterns and problems, *J. Non-Cryst. Solids*, 1991, **131–133**, 13–31.

20 K. Geirhos, P. Lunkenheimer, M. Michl, D. Reuter and A. Loidl, Communication: Conductivity enhancement in plastic-crystalline solid-state electrolytes, *J. Chem. Phys.*, 2015, **143**, 081101.

21 E. I. Cooper and C. A. Angell, Ambient temperature plastic crystal fast ion conductors (PLICFICS), *Solid State Ionics*, 1986, **18–19**, 570–576.

22 M. Jansen, Volume Effect or Paddle-Wheel Mechanism—Fast Alkali-Metal Ionic Conduction in Solids with Rotationally Disordered Complex Anions, *Angew. Chem., Int. Ed. Engl.*, 1991, **30**, 1547–1558.

23 D. Reuter, P. Lunkenheimer and A. Loidl, Plastic-crystalline solid-state electrolytes: Ionic conductivity and orientational dynamics in nitrile mixtures, *J. Chem. Phys.*, 2019, **150**, 244507.

24 Z. Zhang and L. F. Nazar, Exploiting the paddle-wheel mechanism for the design of fast ion conductors, *Nat. Rev. Mater.*, 2022, **7**, 389–405.

25 P. Derollez, J. Lefebvre and M. Descamps, Neutron diffuse scattering in the plastic phase of succinonitrile, *J. Phys.: Condens. Matter*, 1990, **2**, 9975–9987.

26 G. Cardini, R. Righini and S. Califano, Computer simulation of the dynamics of the plastic phase of succinonitrile, *J. Chem. Phys.*, 1991, **95**, 679–685.

27 S. Das, S. Mitra, J. Combet, R. Mukhopadhyay and A. J. Bhattacharyya, Study of solvent relaxation of pristine succinonitrile and succinonitrile–salt mixtures using quasielastic neutron scattering, *Solid State Ionics*, 2015, **279**, 72–77.

28 L. Van Eijck, A. Best, S. Long, F. Fernandez-Alonso, D. MacFarlane, M. Forsyth and G. Kearley, Localized Relaxational Dynamics of Succinonitrile, *J. Phys. Chem. C*, 2009, **113**, 15007–15013.

29 W. V. Edwards, A. Berko, A. N. Blacklocks, S. L. P. Savin and A. V. Chadwick, Ionic Transport and Structure in Doped Plastically Crystalline Solids, *Z. Phys. Chem.*, 2012, **226**, 409–420.

30 P. S. Whitfield, A. Abouimrane and I. J. Davidson, In-situ XRD study of the succinonitrile–lithium bis(trifluoromethylsulfonyl) imide (LiTFSI) phase diagram, *Solid State Ionics*, 2010, **181**, 740–744.

31 Y. Shen, G.-H. Deng, C. Ge, Y. Tian, G. Wu, X. Yang, J. Zheng and K. Yuan, Solvation structure around the Li^+ ion in succinonitrile–lithium salt plastic crystalline electrolytes, *Phys. Chem. Chem. Phys.*, 2016, **18**, 14867–14873.

32 S. Hore, R. Dinnebier, W. Wen, J. Hanson and J. Maier, Structure of Plastic Crystalline Succinonitrile: High-Resolution in situ Powder Diffraction, *Z. Anorg. Allg. Chem.*, 2009, **635**, 88–93.

33 R. Sasaki, M. Moriya, Y. Watanabe, K. Nishio, T. Hitosugi and Y. Tateyama, peculiarly fast Li-ion conduction mechanism in a succinonitrile-based molecular crystal electrolyte: a molecular dynamics study, *J. Mater. Chem. A*, 2021, **9**, 14897–14903.

34 M. Zachariah, M. Romanini, P. Tripathi, M. Barrio, J. L. Tamarit and R. Macovez, Self-Diffusion, Phase Behavior, and Li^+ Ion Conduction in Succinonitrile-Based Plastic Cocrystals, *J. Phys. Chem. C*, 2015, **119**, 27298–27306.

35 D. V. Nickel, H. Bian, J. Zheng and D. M. Mittleman, Terahertz Conductivity and Hindered Molecular Reorientation of Lithium Salt Doped Succinonitrile in its Plastic Crystal Phase, *J. Infrared, Millimeter, Terahertz Waves*, 2014, **35**, 770–779.

36 K. Tanaka, Y. Tago, M. Kondo, Y. Watanabe, K. Nishio, T. Hitosugi and M. Moriya, High Li-Ion Conductivity in $Li\{N(SO_2F)_2\}(NCCH_2CH_2CN)_2$ Molecular Crystal, *Nano Lett.*, 2020, **20**, 8200–8204.

37 S. K. Davidowski, A. R. Young-Gonzales, R. Richert, J. L. Yarger and C. A. Angell, Relation of Ionic Conductivity to Solvent Rotation Times in Dinitrile Plastic Crystal Solvents, *J. Electrochem. Soc.*, 2020, **167**, 070553.

Open Access Article. Published on 16 March 2023. Downloaded on 12/6/2025 1:20:20 PM.
This article is licensed under a Creative Commons Attribution 3.0 Unported Licence.

38 R. Böhmer, K. R. Jeffrey and M. Vogel, Solid-state lithium NMR with applications to the translational dynamics in ion conductors, *Prog. Nucl. Magn. Reson. Spectrosc.*, 2007, **50**, 87–174.
39 A. Kuhn, M. Kunze, P. Sreeraj, H.-D. Wiemhöfer, V. Thangadurai, M. Wilkening and P. Heitjans, NMR relaxometry as a versatile tool to study Li ion dynamics in potential battery materials, *Solid State Nucl. Magn. Reson.*, 2012, **42**, 2–8.
40 C. Vinod Chandran and P. Heitjans, Solid-State NMR Studies of Lithium Ion Dynamics Across Materials Classes, *Annu. Rep. NMR Spectrosc.*, 2016, **89**, 1–102.
41 O. Pecher, J. Carretero-González, K. J. Griffith and C. P. Grey, Materials' Methods: NMR in Battery Research, *Chem. Mater.*, 2016, **29**, 213–242.
42 S. Haber and M. Leskes, What Can We Learn from Solid State NMR on the Electrode–Electrolyte Interface?, *Adv. Mater.*, 2018, **30**, 1706496.
43 R. Böhmer, M. Storek and M. Vogel, NMR studies of ionic dynamics in solids, in *Modern Methods in Solid-State NMR: A Practitioner's Guide*, ed. P. Hodgkinson, Royal Society of Chemistry, 2018, ch. 7, pp. 193–230.
44 A. Golemme, S. Zamir, R. Poupko, H. Zimmermann and Z. Luz, Selfdiffusion in the plastic phase of succinonitrile by 2H NMR quadrupole echo train, *Mol. Phys.*, 1994, **81**, 569–678.
45 R. Böhmer, G. Diezemann, G. Hinze and E. Rössler, Dynamics of supercooled liquids and glassy solids, *Prog. Nucl. Magn. Reson. Spectrosc.*, 2001, **39**, 191–267.
46 S. K. Davidowski, J. L. Yarger, R. Richert and C. A. Angell, Reorientation Times for Solid State Electrolyte Solvents and Electrolytes from NMR Spin Lattice Relaxation Studies, *J. Phys. Chem. Lett.*, 2020, **11**, 3301–3304.
47 W. J. Orville-Thomas, Tables of Experimental Dipole Moments, *J. Mol. Struct.*, 1977, **36**, 165–171.
48 S. Lansab, P. Münzner, H. Zimmermann and R. Böhmer, Deuteron nuclear magnetic resonance and dielectric studies of molecular reorientation and charge transport in succinonitrile-glutaronitrile plastic crystals, *J. Non-Cryst. Solids: X*, 2022, **14**, 100097.
49 T. Bauer, M. Köhler, P. Lunkenheimer, A. Loidl and C. A. Angell, Relaxation Dynamics and Ionic Conductivity in a Fragile Plastic Crystal, *J. Chem. Phys.*, 2010, **133**, 144509.
50 M. Götz, T. Bauer, P. Lunkenheimer and A. Loidl, Supercooled-liquid and plastic-crystalline state in succinonitrile-glutaronitrile mixtures, *J. Chem. Phys.*, 2014, **140**, 094504.
51 D. Massiot, F. Fayon, M. Capron, I. King, S. Le Calvé, B. Alonso, J.-O. Durand, B. Bujoli, Z. Gan and G. Hoatson, Modelling one- and two-dimensional solid-state NMR spectra, *Magn. Reson. Chem.*, 2001, **40**, 70–76.
52 D. H. Wu, A. D. Chen and C. S. Johnson, An Improved Diffusion-Ordered Spectroscopy Experiment Incorporating Bipolar-Gradient Pulses, *J. Magn. Reson.*, 1995, **115**, 260–264.
53 R. Brand, P. Lunkenheimer and A. Loidl, Relaxation dynamics in plastic crystals, *J. Chem. Phys.*, 2002, **116**, 10386–10401.
54 C. J. F. Böttcher and P. Bordewijk, *Theory of Electric Polarization II: Dielectrics in Time-Dependent Fields*, Elsevier, Amsterdam, 1978.
55 F. Kremer and A. Schönhals, *Broadband Dielectric Spectroscopy*, Springer, Berlin, Heidelberg, 2003.
56 N. Bloembergen, E. M. Purcell and R. V. Pound, Relaxation Effects in Nuclear Magnetic Resonance Absorption, *Phys. Rev.*, 1948, **73**, 679–712.
57 A. Abragam, *The Principles of Nuclear Magnetism*, Oxford University Press, Oxford, 1961, p. 456.
58 M. J. Zuriaga, R. Hallsworth, R. L. Armstrong, G. A. Monti and C. A. Martín, An NQR and NMR study of solid trichlorofluoromethane, *J. Magn. Reson.*, 1992, **99**, 56–65.
59 M. Bee, R. E. Lechner, J. P. Amoureux and R. Fouret, Temperature dependence of rotational isomerisation and molecular reorientation rates in plastic succinonitrile, *J. Phys. C: Solid State Phys.*, 1983, **16**, 4973–4983.
60 P. A. Beckmann, Spectral densities and nuclear spin relaxation in solids, *Phys. Rep.*, 1988, **171**, 85–128.
61 H. W. Spiess, in Rotation of Molecules and Nuclear Spin Relaxation, *Dynamic NMR Spectroscopy*, Springer, Berlin, 1978.
62 G. Diezemann and H. Sillescu, Dipolar interactions in deuteron spin systems. II. Transverse relaxation, *J. Chem. Phys.*, 1995, **103**, 6385–6393.
63 H. Nelson, A. Ihrig, R. Kahlau, P. Kibies, S. M. Kast and R. Böhmer, Dielectric and deuteron magnetic resonance studies of guest reorientation and defect dynamics in six clathrate hydrates with ring-type guests, *J. Non-Cryst. Solids*, 2015, **407**, 431–440.
64 H. Mehrer, *Diffusion in Solids*, Springer, Berlin, Heidelberg, 2009.
65 R. Rohan, T.-C. Kuo, J.-H. Lin, Y.-C. Hsu, C.-C. Li and J.-T. Lee, Dinitrile–Mononitrile-Based Electrolyte System for Lithium-Ion Battery Application with the Mechanism of Reductive Decomposition of Mononitriles, *J. Phys. Chem. C*, 2016, **120**, 6450–6458.
66 B. Geil, Measurement of translational molecular diffusion using ultrahigh magnetic field gradient NMR, *Concepts Magn. Reson.*, 1998, **10**, 299–321.
67 E. O. Stejskal and J. E. Tanner, Spin Diffusion Measurements: Spin Echoes in the Presence of a Time-Dependent Field Gradient, *J. Chem. Phys.*, 1965, **42**, 288–292.
68 J. C. Dyre, P. Maass, B. Roling and D. L. Sidebottom, Fundamental questions relating to ion conduction in disordered solids, *Rep. Prog. Phys.*, 2009, **72**, 046501.
69 C. Gainaru, S. Ahlmann, L. S. Röwekamp, K. Moch, S. P. Bierwirth and R. Böhmer, Rheology based estimates of self- and collective diffusivities in viscous liquids, *J. Chem. Phys.*, 2021, **155**, 011101.
70 J. T. Edward, Molecular Volumes and Stokes-Einstein Equation, *J. Chem. Educ.*, 1970, **47**, 261–270.
71 M. Storek, K. R. Jeffrey and R. Böhmer, Local-field approximation of homonuclear dipolar interactions in ^{7}Li-NMR:

 This journal is © the Owner Societies 2023

Density-matrix calculations and random-walk simulations tested by echo experiments on borate glasses, *Solid State Nucl. Magn. Reson.*, 2014, **59–60**, 8–19.
72 M. Michl, T. Bauer, P. Lunkenheimer and A. Loidl, Nonlinear dielectric spectroscopy in a fragile plastic crystal, *J. Chem. Phys.*, 2016, **144**, 114506.
73 A. Lundén, On the paddle-wheel mechanism for cation conduction in lithium sulphate, *Z. Naturforsch., A: Phys. Sci.*, 1995, **11**, 1067–1076.
74 Z. Xu and Y. Xia, Progress, challenges and perspectives of computational studies on glassy superionic conductors for solid-state batteries, *J. Mater. Chem. A*, 2022, **10**, 11854–11880.

Open Access Article. Published on 16 March 2023. Downloaded on 12/6/2025 1:20:20 PM.
This article is licensed under a Creative Commons Attribution 3.0 Unported Licence.